 CMC, vol.29, no.1, pp.15-39, 2012

Nonlinear Dynamic Analysis of Three-Dimensional Elasto-Plastic Solids by the Meshless Local Petrov-Galerkin (MLPG) Method

A. Rezaei Mojdehi[1,2], A. Darvizeh[3] and A. Basti[2]

Abstract: The meshless local Petrov-Galerkin approach is proposed for the nonlinear dynamic analysis of three-dimensional (3D) elasto-plastic problems. Galerkin weak-form formulation is applied to derive the discrete governing equations. A weak formulation for the set of governing equations is transformed into local integral equations on local sub-domains by using a unit test function and local weak-form formulation in three dimensional continua for the general dynamic problems is derived. Three dimensional Moving Least-Square (MLS) approximation is considered as shape function to approximate the field variable of scattered nodes in the problem domain. Normality hypothesis of plasticity is adopted to define the stress-strain relation in elasto-plastic analysis and the unknown plastic multiplier is obtained by the consistency condition. Von Mises yield criterion in three dimensional space is used as a yield function to determine whether the material has yielded. The Newmark time integration method in an incremental form is used to solve the final system of nonlinear second order Ordinary Differential Equations (ODEs). Several numerical examples are given to demonstrate the accuracy and effectiveness of the present numerical approach.

Keywords: Meshless Local Petrov-Galerkin method, Three Dimensional Moving Least Square approximation, Nonlinear Dynamic Analysis, Normality Hypothesis of Plasticity.

1 Introduction

For realistic simulation of engineering phenomena, exact modeling of the material behaviour to obtain a reliable and accurate design is necessary. In this regard, con-

[1] Wind Turbines Technology Development Center, Niroo Research Institute, Tehran, Iran
[2] Department of Mechanical engineering, Faculty of Engineering, The University of Guilan, Iran
[3] Department of Mechanical Engineering, Faculty of Engineering, Islamic Azad University, Anzali Branch, Bandar-e Anzali, Iran

sidering nonlinearities, due to inelasticity of material, play an important role in accurate response of engineering structures under large dynamic loading conditions. In recent decades, significant researches have been carried out to investigate nonlinear behaviour of structures under transient dynamic loading with applications to nuclear reactors, ship structures and multistory buildings subjected to earthquake loadings.

Despite the widespread applications of finite element method (FEM) in solution of engineering problems, new advanced methods, such as meshless approaches, have attracted considerable attention owing to their high adaptivity, low cost to prepare input data for numerical analysis and some advantages which overcome difficulties associated with the FEM. A variety of these meshless methods have been developed which include element-free Galerkin method [Belytschko, Lu and Gu (1994)], the reproducing kernel particle method [Liu, W. K., Jun and Zhang (1995)], hp-clouds [Duarte and Oden (1996)], the partition of unity method [Babuska and Melenk (1997)], meshless Galerkin using radial basis functions [Wendland (1995)], the diffuse element [Nayroles, Touzot and Villon (1992)], the natural element [Sukumar, Moran and Belytschko (1998)], the smoothed particle hydrodynamics [Lucy (1977)], the collocation technique employing radial basis functions [Fasshauer (1997)] and the modified smoothed particle hydrodynamics [Zhang, G. M. and Batra (2004)]. Some of them are derived from weak form formulation on global domain in which require the generation of background cells for the integration of the weak form and the others, are based on local weak form and no cells are required for integration of governing equations.

The Meshless Local Petrov–Galerkin (MLPG) method developed by Atluri et al. [(1998); (1999); (2002b); (2002a)] is a truly meshless method which is based on the local weak rather than the global weak forms. In the MLPG method, the trial and test functions are totally independent and can be chosen in different functional spaces and domain sizes. Based on the concept of the MLPG, six different methods have been introduced, which are labeled as MLPG1–MLPG6 [Atluri and Shen (2002b)] . Difference between These six methods is due to the type of test function considered in the weak formulation. The MLPG methods have been used to solve various problems in wide range of applications, including the works on elasto-statics [Atluri and Zhu (2000)], elasto- dynamics [Batra and Ching (2002)], fluid mechanics [Lin and Atluri (2001)], convection–diffusion problems [Lin and Atluri (2000)], thermoelasticity [Sladek, Sladek and Atluri (2001)], beam problems [Atluri, Cho and Kim (1999); Gu and Liu (2001)], plate problems [Gu and Liu (2001); Long, S. and Atluri (2002); Qian, L. F, Batra and Chen (2003); Soric, Li, Jarak and Atluri (2004); Li, Soric, Jarak and Atluri (2005); Sladek, Sladek, Krivacek, Wen and Zhang (2007); Xiao, Batra, Gilhooley, Gillespie Jr. and McCarthy

(2007)], fracture mechanics [Kim and Atluri (2000); Ching and Batra (2001)], strain gradient theory [Tang, Shen and Atluri (2003)] and FGM problems [Qian, L. F., Batra and Chena (2004); Ching and Yen (2005); Sladek, sladek and Zhang (2005); Ching and Yen (2006); Gilhooley, Batra, Xiao, McCarthy and Gillespie Jr. (2007); Sladek, Sladek and Solek (2009); Rezaei Mojdehi, Darvizeh, Basti and Rajabi (2011)] . All of these wide ranges of applications demonstrate that the MLPG method is one of the most promising alternative methods for computational mechanics.

The majority of papers in which MLPG methods are applied are confined to the elastic analysis. There are a few works carried out with MLPG method for analysis of elasto-plastic materials and material nonlinearities, which most of them are limited to two-dimensional analysis. Zhang et al. (2006) presented two-dimensional large deformation analysis of hyper-elastic and elasto-plastic materials based on MLPG method. Gu et al. (2007) extended MLPG method for two-dimensional analysis of material nonlinear problems based on deformation theory of plasticity. Long et al. (2008) developed MLPG method for elasto-plastic fracture problems. Heaney et al. (2009) demonstrated modeling of elasto-plastic materials by the MLPG method with application to problems in geomechanics. Soares et al. (2009) presented nonlinear dynamic analysis of two-dimensional solids based on Newmark/Newton-Raphson method. After many pioneering research studies were successfully performed based on 2D analysis, the MLPG methods, because of its distinct advantages over the element-based methods Atluri and Shen (2002b); (2002a); Han and Atluri (2004), are becoming more attractive for solving 3D problems. After a search of published literature, it has been revealed that there are only two papers in which performed three-dimensional analysis of material nonlinear problems by the MLPG methods. Han et al. (2005) developed MLPG mixed finite volume method for the large deformation analysis of static and dynamic problems with application to 3D high speed impact problems. Rezaei Mojdehi et al. (2011) also extended MLPG method for static analysis of 3D elasto-plastic problems based on deformation theory of plasticity. Up to now, to the authors' knowledge, there is no work dealing with the transient dynamic analysis of 3D elasto-plastic solids by the MLPG methods. The purpose of the present paper is to fill this apparent void by the implementation of MLPG method in 3D dynamic elasto-plastic problems. Accordingly, meshless local Petrov-Galerkin method is extended for the nonlinear analysis of 3D elasto-plastic problems under dynamic loading.

The organization of the present paper is as follows: In Section 2, local weak-form formulation of the governing equilibrium equations in three dimensional continua for the general dynamic problems is derived. Nodal points are distributed in the 3D analyzed domain and each node is surrounded by a cubic sub-domain to which a

local integral equation is applied. Three dimensional Moving Least-Square (MLS) approximation is presented as shape function to approximate the field variable of scattered nodes in the problem domain. Fourth-order spline function is used as the weight function as well as the test function. In Section 3, stress-strain relation in elasto-plasticity problems is represented based on normality hypothesis of plasticity and the unknown plastic multiplier is obtained by the consistency condition. Von Mises yield criterion in three dimensional space is used as a yield function to determine whether the material has yielded. In Section 4, the obtained equations are discretized by the MLS shape function and the final Ordinary Differential Equations (ODEs) of the problem domain are demonstrated. The Newmark time integration method in an incremental form is used to solve the obtained system of nonlinear second order ODEs. Several numerical examples are presented to illustrate the accuracy and effectiveness of the present meshless formulation.

2 MLPG formulation for 3D dynamic problems

Based on equilibrium equations in three-dimensional continua, for a domain of the volume Ω, which is bounded by the surface Γ, we have;

$$\sigma_{ij,j}(\mathbf{x},t)+b_i(\mathbf{x},t)=\rho\ddot{u}_i(\mathbf{x},t), \qquad in\ \Omega \tag{1}$$

where $\sigma_{ij,j}(\mathbf{x},t)$ are the components of the symmetric stress tensor which correspond to the displacement field $u_i(\mathbf{x},t)$, $b_i(\mathbf{x},t)$ are the body force, ρ is the mass density and $\ddot{u}_i(\mathbf{x},t)$ the acceleration. The indices *i, j* which take the values 1, 2 and 3 refer to the coordinates *x, y, z* on the boundary Γ, respectively. The following boundary conditions are considered;

$$u_i(\mathbf{x},t)=\overline{u}_i(\mathbf{x},t), \qquad on\ \ \Gamma_u \tag{2a}$$

$$t_i(\mathbf{x},t)=\sigma_{ij}(\mathbf{x},t)n_j(\mathbf{x})=\bar{t}_i(\mathbf{x},t), \qquad on\ \ \Gamma_t \tag{2b}$$

where $\overline{u}_i(\mathbf{x},t)$ and $\bar{t}_i(\mathbf{x},t)$ are the prescribed displacements and surface tractions, on the displacement boundary Γ_u and on the traction boundary Γ_t, respectively. $n_j(\mathbf{x})$ are the components of a unit outward normal to the global boundary Γ.

The corresponding initial conditions are;

$$u_i(\mathbf{x},t)\big|_{t=0}=u_i(\mathbf{x},0) \qquad \mathbf{x}\in\Omega \tag{3a}$$

$$\dot{u}_i(\mathbf{x},t)\big|_{t=0}=\dot{u}_i(\mathbf{x},0) \qquad \mathbf{x}\in\Omega \tag{3b}$$

where $u_i(\mathbf{x},0)$ and $\dot{u}_i(\mathbf{x},0)$ are the values of the initial displacements and velocities, respectively.

The weak form of governing equations can be obtained over the local sub-domains, which are located entirely inside the global domain Ω. The local sub-domains may overlap with each other and must cover the whole global domain. Various arbitrary shapes, with different sizes, such as spheres, cubes and ellipsoids can be chosen as sub-domains in 3D domains. In the present work, cubic domains are considered as local sub-domain and support domain which can be seen in Fig. 1.

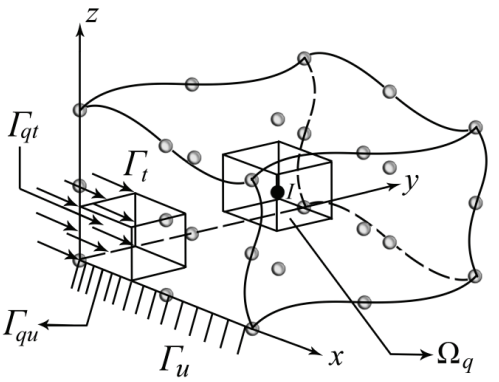

Figure 1: Local sub-domains used in the MLPG method

2.1 Local weak form of 3D solids

Based on the local Petrov-Galerkin approaches, a generalized local weak form of the equilibrium equation over a local sub-domain Ω_q, can be written as;

$$\int_{\Omega q} \left(\sigma_{ij,j}(\mathbf{x},t) + b_i(\mathbf{x},t) - \rho \ddot{u}_i(\mathbf{x},t)\right)_i(\mathbf{x}) d\Omega = 0 \tag{4}$$

herein $u_i(\mathbf{x},t)$ is the trial function describing the displacement field, while $v_i(\mathbf{x})$ is the test function.

Unlike the conventional Galerkin method in which the trial and test functions are chosen from the same space, the Petrov-Galerkin method uses the trial and the test functions from different spaces. In particular, the test functions do not need to vanish on the boundary where the essential boundary conditions are specified. By applying the divergence theorem, Eq. 4 may be rewritten as;

$$\sigma_{ij,j}(\mathbf{x},t)\, v_i(\mathbf{x}) = \left(\sigma_{ij}(\mathbf{x},t)\, v_i(\mathbf{x})\right)_{,j} - \sigma_{ij}(\mathbf{x},t)\, v_{i,j}(\mathbf{x}) \tag{5}$$

by imposing the natural boundary conditions in Eq. 2b one obtains;

$$\int_{\Gamma_{qi}} t_i(\mathbf{x},t)v_i(\mathbf{x})d\Gamma + \int_{\Gamma_{qu}} t_i(\mathbf{x},t)v_i(\mathbf{x})d\Gamma + \int_{\Gamma_{qt}} \bar{t}_i(\mathbf{x},t)v_i(\mathbf{x})d\Gamma - \int_{\Omega_q} (\sigma_{ij}(\mathbf{x},t)v_{i,j}(\mathbf{x}) + \rho\ddot{u}_i(\mathbf{x},t)v_i(\mathbf{x}) - b_i(\mathbf{x},t)v_i(\mathbf{x}))\, d\Omega = 0 \quad (6)$$

where Ω_q has composed by three parts, i.e. $\Gamma_q = \Gamma_{qi} \cup \Gamma_{qu} \cup \Gamma_{qt}$, in which Γ_{qi} is the internal boundary of the local sub-domain, which does not intersect with the global boundary Γ; Γ_{qt} is the part of the natural boundary that intersects with the local sub-domain and Γ_{qu} is the part of the essential boundary that intersects with the local sub-domain. Fig. 1, shows the local sub-domain used in the MLPG method.

Eq. 7 can be rewritten as;

$$\int_{\Omega_q} (\sigma_{ij}(\mathbf{x},t)v_{i,j}(\mathbf{x}) + \rho\ddot{u}_i(\mathbf{x},t)v_i(\mathbf{x}))\, d\Omega - \int_{\Gamma_{qi}} t_i(\mathbf{x},t)v_i(\mathbf{x})d\Gamma - \int_{\Gamma_{qu}} t_i(\mathbf{x},t)v_i(\mathbf{x})d\Gamma = \int_{\Gamma_{qt}} \bar{t}_i(\mathbf{x},t)v_i(\mathbf{x})d\Gamma + \int_{\Omega_q} b_i(\mathbf{x},t)v_i(\mathbf{x})d\Omega \quad (7)$$

which represent a set of three equations for each local sub-domain. In the present implementation, the local domain is chosen as a cube, centered at a node $\mathbf{x}_i$. The test function $v_i(\mathbf{x})$ is chosen such that it is positive inside the local sub-domain Ω_q and vanishes outside of Ω_q.

2.2 3D approximation using Moving Least Square (MLS) approximation

The trial function for the displacement at each point can be approximated by the MLS shape function.

The MLS approximation of $u(\mathbf{x},\ t)$ is defined at $\mathbf{x}$ as;

$$u^h(\mathbf{x},t) = \sum_{i=1}^{m} p_i(\mathbf{x})\, a_i(\mathbf{x},t) = \mathbf{p}^{\mathrm{T}}(\mathbf{x})\,\mathbf{a}(\mathbf{x},t) \qquad \forall \mathbf{x} \in \Omega \quad (8)$$

where $\mathbf{p}^T(\mathbf{x}) = [p_1(\mathbf{x}), p_2(\mathbf{x}), \ldots, p_m(\mathbf{x})]$ is a vector of complete basis functions of order m and $\mathbf{a}(\mathbf{x})$ is a vector containing the coefficients $a_i(\mathbf{x})$, $i = 1,\ 2,\ \ldots,\ m$, which are functions of the space coordinates $\mathbf{x} = [x,\ y,\ z]^T$. In 3D problems, the linear basis is defined as;

$$\mathbf{p}^{\mathrm{T}}(\mathbf{x}) = [1, x, y, z];\ \ m = 4 \quad (9)$$

and the quadratic basis is defined as;

$$\mathbf{p}^{\mathrm{T}}(\mathbf{x}) = \left[1, x, y, z, x^2, y^2, z^2, xy, yz, xz\right];\ m = 10 \quad (10)$$

The coefficient vector function $a_i(\mathbf{x})$ is obtained by minimizing a weighted discrete L_2 norm, which is defined as;

$$J(\mathbf{x}) = \int_{I=1}^{N} \mathrm{w}_I(\mathbf{x}) \left[\mathbf{p}^{\mathrm{T}}(\mathbf{x}_I)\mathbf{a}(\mathbf{x},t) - \hat{u}^I(t)\right]^2 \tag{11}$$

where $\hat{u}^I(t)$ are the fictitious nodal values and $\mathrm{w}_I(\mathbf{x})$ is the weight function associated with the node I. N is the number of nodes in the support domain for which the weight function $\mathrm{w}_I(\mathbf{x}) > 0$ and $\mathbf{x}_I$ denotes the value of $\mathbf{x}$ at node I. A fourth-order spline weight function is considered in the present work. This weight function corresponding to node I for a one-dimensional domain may be written as;

$$w_I(x) = \begin{cases} 1 - 6\left(\frac{d_I(x)}{r_I^x}\right)^2 + 8\left(\frac{d_I(x)}{r_I^x}\right)^3 - 3\left(\frac{d_I(x)}{r_I^x}\right)^4 & 0 \le d_I(x) \le r_I^x \\ 0 & d_I(x) > r_I^x \end{cases} \tag{12}$$

where $d_I(x) = x - x_I$ is the distance from node $\mathbf{x}_I$ to point $\mathbf{x}$ in x direction; while $r_I(x)$ is the size of the support for the weight function $w_I(x)$ defined as $r_I^x = \alpha_s d_I^x$ which the weight function $w_I(x)$ associated with node $\mathbf{x}_I$ is non-zero and α_s is the dimensionless size of the support domain. Using the cubic support domain, the weight function for the 3D problem can be obtained by a simple extension of the one-dimensional function of Eq. 13 as follows;

$$\mathrm{w}_I(\mathbf{x}) = \mathrm{w}_I(x,y,z) = w_I(x)\, w_I(y)\, w_I(z) \tag{13}$$

where functions $w_I(y)$ and $w_I(z)$ are obtained by replacing x with y and z in Eq. 13, respectively. In this regard, the parameters $d_I(y) = y - y_I$ and $d_I(z) = z - z_I$ are the distances from node $\mathbf{x}_I$ to point $\mathbf{x}$ in y and z direction, respectively.

The stationary condition of J in Eq. 12 with respect to $\mathbf{a}(\mathbf{x},t)$,

$$\partial J / \partial \mathbf{a} = 0 \tag{14}$$

leads to the following linear relation between fictitious ($\widehat{\mathbf{u}}$) and approximated (u^h) nodal displacements.

$$u^h(\mathbf{x},t) = \int_{I=1}^{N} \Phi^I(\mathbf{x})\, \hat{u}^I(t) = \mathbf{\Phi}^{\mathrm{T}}(\mathbf{x})\, \widehat{\mathbf{u}}(t) \tag{15}$$

where $\mathbf{\Phi}^T(\mathbf{x})$ can then be introduced as the shape function associated with the nodes and is given as;

$$\mathbf{\Phi}^T(\mathbf{x}) = \mathbf{P}^{\mathrm{T}}(\mathbf{x})\, \mathbf{A}^{-1}(\mathbf{x})\, \mathbf{B}(\mathbf{x}) \tag{16}$$

where,

$$\mathbf{A}(\mathbf{x}) = \int_{I=1}^{N} \mathrm{w}_I(\mathbf{x})\mathbf{p}(\mathbf{x}_I)\,\mathbf{p}^{\mathrm{T}}(\mathbf{x}_I) = \mathbf{P}^{\mathbf{T}}\mathbf{W}P \tag{17}$$

$$\mathbf{B}(\mathbf{x}) = [\mathrm{w}_1(\mathbf{x})\,\mathbf{p}(\mathbf{x}_1),\ \mathrm{w}_2(\mathbf{x})\,\mathbf{p}(\mathbf{x}_2),\ \ldots,\ \mathrm{w}_N(\mathbf{x})\,\mathbf{p}(\mathbf{x}_{\mathrm{N}})] = \mathbf{P}^{\mathbf{T}}\mathbf{W} \tag{18}$$

herein,

$$\mathbf{P} = \begin{bmatrix} \mathbf{p}^{\mathrm{T}}(\mathbf{x}_1) \\ \mathbf{p}^{\mathrm{T}}(\mathbf{x}_2)\vdots \\ \mathbf{p}^{\mathrm{T}}(\mathbf{x}_{\mathrm{N}}) \end{bmatrix}_{N\times m} \tag{19}$$

and,

$$\mathbf{W} = \begin{pmatrix} \mathrm{w}_1(\mathbf{x}) & \cdots & 0 \\ \vdots & \ddots & \vdots \\ 0 & \cdots & \mathrm{w}_N(\mathbf{x}) \end{pmatrix}_{N\times N} \tag{20}$$

The partial derivatives of the trial function are presented as follows;

$$u^h_{,x}(\mathbf{x},t) = \int_{I=1}^{N} \Phi^I_{,x}(\mathbf{x})\,\hat{u}^I(t) \tag{21}$$

where $\Phi^I_{,x}$ are derivatives of the MLS shape function and can be obtained as;

$$\Phi^I_{,x}(\mathbf{x}) = \int_{j=1}^{m} \left[p_{j,x}\left(\mathbf{A}^{-1}\mathbf{B}\right)_{jI} + p_j\left(\mathbf{A}^{-1}\mathbf{B}_{,x} + \mathbf{A}^{-1}_{,x}\mathbf{B}\right)_{jI} \right] \tag{22}$$

where $\mathbf{A}^{-1}_{,x} = -\mathbf{A}^{-1}\mathbf{A}_{,x}\mathbf{A}^{-1}$ represents the derivative of the inverse of matrix $\mathbf{A}$ with respect to x.

2.3 Test function

Atluri and Shen (2002b) have proposed six different choices for test functions and labeled the corresponding formulations as MLPG1 through MLPG6. Here we take the test function to be a fourth-order spline weight function. The corresponding MLPG formulation is called MLPG1. Cubic sub-domain is also chosen for the support of the test function. The test function for the cubic sub-domain is constructed following the same procedure as mentioned in the previous section for constructing

the weight function. Therefore, the test function for MLPG1 in node $\mathbf{x}_I$ is defined as;

$$\begin{aligned} v_i(\mathbf{x}) &= v_i(x)\, v_i(y)\, v_i(z) \\ &= \begin{cases} 1-6\left(\frac{d_I(\mathbf{x})}{r_q^x}\right)^2+8\left(\frac{d_I(\mathbf{x})}{r_q^x}\right)^3-3\left(\frac{d_I(\mathbf{x})}{r_q^x}\right)^4 & 0\le d_I(\mathbf{x})\le r_q^x \\ 0 & d_I(\mathbf{x})>r_q^x \end{cases} \end{aligned} \tag{23}$$

where $d_I(\mathbf{x})=\mathbf{x}-\mathbf{x}_I$ and r_q^x is the size of the support for the test function v_I defined as $r_q^x=\alpha_q d_I^x$ which the test function $v_i(\mathbf{x})$ associated with node $\mathbf{x}_I$ is non-zero and α_q is the dimensionless size of the support for the test function domain.

3 Stress-strain relation in elasto-plasticity

According to the classical additive decomposition of strain, total strain can be written as summation of elastic strain and plastic one in the incremental form as follow;

$$d\boldsymbol{\varepsilon}=d\boldsymbol{\varepsilon}^e+d\boldsymbol{\varepsilon}^p \tag{24}$$

Elastic strain is related to the stress tensor by Hook's law for isotropic material as;

$$d\boldsymbol{\sigma}=\mathbf{D}d\boldsymbol{\varepsilon}^e=\mathbf{D}\left(d\boldsymbol{\varepsilon}-d\boldsymbol{\varepsilon}^p\right) \tag{25}$$

where $\mathbf{D}$ is the three-dimensional elastic stress-strain matrix as;

$$\mathbf{D}=D_0\begin{bmatrix} 1 & \frac{\nu}{1-\nu} & \frac{\nu}{1-\nu} & 0 & 0 & 0 \\ \frac{\nu}{1-\nu} & 1 & \frac{\nu}{1-\nu} & 0 & 0 & 0 \\ \frac{\nu}{1-\nu} & \frac{\nu}{1-\nu} & 1 & 0 & 0 & 0 \\ 0 & 0 & 0 & \frac{1-2\nu}{2(1-\nu)} & 0 & 0 \\ 0 & 0 & 0 & 0 & \frac{1-2\nu}{2(1-\nu)} & 0 \\ 0 & 0 & 0 & 0 & 0 & \frac{1-2\nu}{2(1-\nu)} \end{bmatrix} \tag{26}$$

$$D_0=\frac{E(1-\nu)}{(1+\nu)(1-2\nu)} \tag{27}$$

In which E and ν are Young's modulus and Poisson's ratio, respectively.

Based on normality hypothesis of plasticity, the increment in the plastic strain tensor is in a direction which is normal to the tangent to the yield surface at the load point. It can be written in terms of the yield function, f, as;

$$\mathrm{d}\boldsymbol{\varepsilon}^p=d\lambda\frac{\partial \mathrm{f}}{\partial\boldsymbol{\sigma}} \tag{28}$$

where von Mises yield function can be defined as;

$$\mathrm{f} = \sigma_e - \sigma_y = \left(\frac{3}{2}\acute{\sigma}_{ij}\acute{\sigma}_{ij}\right)^{1/2} - \sigma_y \tag{29}$$

where σ_e, $\acute{\sigma}_{ij}$ and σ_y are effective stress, deviatoric stress and yield stress, respectively. $d\lambda$ is called plastic multiplier and can be obtained by consistency condition. In general case, the yield stress in Eq. 30 is a function of effective plastic strain, p, which can be written in the incremental form as;

$$dp = \left(\frac{2}{3}d\varepsilon_{ij}^{p}\varepsilon_{ij}^{p}\right)^{1/2} \tag{30}$$

Therefore, the yield criterion for the plastic deformation can be written as;

$$\mathrm{f}(\boldsymbol{\sigma},\ p) = 0 \tag{31}$$

The consistency condition for an incremental change in stress and effective plastic strain is defined as;

$$\mathrm{f}(\boldsymbol{\sigma} + d\boldsymbol{\sigma},\ p + dp) = 0 \tag{32}$$

We can expand this as;

$$\mathrm{f}(\boldsymbol{\sigma} + d\boldsymbol{\sigma},\ p + dp) = \mathrm{f}(\boldsymbol{\sigma},\ p) + \frac{\partial f}{\partial \boldsymbol{\sigma}}d\boldsymbol{\sigma} + \frac{\partial f}{\partial p}dp \tag{33}$$

By using Eqs. 26-32 we can obtain the plastic multiplier, $d\lambda$, as;

$$d\lambda = \frac{(\partial f/\partial \boldsymbol{\sigma})\,\mathbf{D}d\boldsymbol{\varepsilon}}{(\partial f/\partial \boldsymbol{\sigma})\,\mathbf{D}\,(\partial f/\partial \boldsymbol{\sigma}) - (\partial f/\partial p)\,((2/3)\,(\partial f/\partial \boldsymbol{\sigma})\,(\partial f/\partial \boldsymbol{\sigma}))^{1/2}} \tag{34}$$

Therefore, by having $d\lambda$ from Eq. 35, the increment in plastic strain tensor can be obtained.

4 Discretization and time integration

The discretization of the problem's geometry is performed by the nodes located on the 3D problem domain. By using the test function in the MLPG method, only three linear equations of $\hat{u}$ will yield for each point and/or its local domains. The nodal variables are three fictitious displacement components in the Cartesian coordinate

system *x, y, z*. Therefore, we need as many local domains Ω_q as the number of nodes in the global domain to obtain as many equations as the number of unknowns.

The stress tensor components σ_{ij} can be written in a Cartesian coordinate system as;

$$\boldsymbol{\sigma}^{\mathrm{T}}(\mathbf{x},t) = [\sigma_x(\mathbf{x},t)\ \ \sigma_y(\mathbf{x},t)\ \ \sigma_z(\mathbf{x},t)\ \ \tau_{xy}(\mathbf{x},t)\ \ \tau_{yz}(\mathbf{x},t)\ \ \tau_{zx}(\mathbf{x},t)] \tag{35}$$

The strain-displacement relation can also be written as;

$$\boldsymbol{\varepsilon}(\mathbf{x},t) = \int_{j=1}^{N} \mathbf{B}_j(\mathbf{x})\mathbf{u}_j(\mathbf{x},t) \tag{36}$$

where $\mathbf{B}(\mathbf{x})$ denotes the strain-displacement matrix obtained by differentiation of the shape function in a three dimensional space;

$$\mathbf{B}(\mathbf{x}) = \begin{bmatrix} \frac{\partial \Phi_1(\mathbf{x})}{\partial x} & 0 & 0 & \dots & \frac{\partial \Phi_N(\mathbf{x})}{\partial x} & 0 & 0 \\ 0 & \frac{\partial \Phi_1(\mathbf{x})}{\partial y} & 0 & \dots & 0 & \frac{\partial \Phi_N(\mathbf{x})}{\partial y} & 0 \\ 0 & 0 & \frac{\partial \Phi_1(\mathbf{x})}{\partial z} & \dots & 0 & 0 & \frac{\partial \Phi_N(\mathbf{x})}{\partial z} \\ \frac{\partial \Phi_1(\mathbf{x})}{\partial y} & \frac{\partial \Phi_1(\mathbf{x})}{\partial x} & 0 & \dots & \frac{\partial \Phi_N(\mathbf{x})}{\partial y} & \frac{\partial \Phi_N(\mathbf{x})}{\partial x} & 0 \\ 0 & \frac{\partial \Phi_1(\mathbf{x})}{\partial z} & \frac{\partial \Phi_1(\mathbf{x})}{\partial y} & \dots & 0 & \frac{\partial \Phi_N(\mathbf{x})}{\partial z} & \frac{\partial \Phi_N(\mathbf{x})}{\partial y} \\ \frac{\partial \Phi_1(\mathbf{x})}{\partial z} & 0 & \frac{\partial \Phi_1(\mathbf{x})}{\partial x} & \dots & \frac{\partial \Phi_N(\mathbf{x})}{\partial z} & 0 & \frac{\partial \Phi_N(\mathbf{x})}{\partial x} \end{bmatrix} \tag{37}$$

The surface traction components $\mathbf{t}(\mathbf{x},t)$ may also be expressed in a vector form by the relation;

$$\mathbf{t}(\mathbf{x},t) = \mathbf{N}(\mathbf{x})\boldsymbol{\sigma}(\mathbf{x},t) \tag{38}$$

which $\mathbf{N}(\mathbf{x})$ is the matrix describing the outward normal on Γ_q,

$$\mathbf{N}(\mathbf{x}) = \begin{bmatrix} n_x(\mathbf{x}) & 0 & 0 & n_y(\mathbf{x}) & 0 & n_z(\mathbf{x}) \\ 0 & n_y(\mathbf{x}) & 0 & n_x(\mathbf{x}) & n_z(\mathbf{x}) & 0 \\ 0 & 0 & n_z(\mathbf{x}) & 0 & n_y(\mathbf{x}) & n_x(\mathbf{x}) \end{bmatrix} \tag{39}$$

By substituting fourth-order spline test function from Eq. 24 into Eq. 8 and by means of Eqs. 16, 26, 37 and 39, governing equations are transformed in the discretized system of ordinary differential equations which may be written in the matrix form as;

$$\mathbf{M}(\mathbf{x})\ddot{\widehat{\mathbf{u}}}(t) + \mathbf{K}(\mathbf{x})\widehat{\mathbf{u}}(t) = \mathbf{F}(\mathbf{x},t) \tag{40}$$

where, $\mathbf{M}(\mathbf{x})$, $\mathbf{K}(\mathbf{x})$ and $\mathbf{F}(\mathbf{x},t)$ are equivalent mass, stiffness and force matrix, respectively which are described in the following;

$$\mathbf{M}_{IJ}(\mathbf{x}) = \int_{J=1}^{N} \int_{\Omega_q} \rho \Phi_J(\mathbf{x}) \mathbf{V}_I(\mathbf{x}) d\Omega \tag{41}$$

$$\mathbf{K}_{IJ}(\mathbf{x}) = \int_{J=1}^{N} \int_{\Omega_q} \widehat{\mathbf{W}}_I^T(\mathbf{x}) \mathbf{D}\mathbf{B}_J(\mathbf{x}) d\Omega - \int_{\Gamma_{qi}} \mathbf{V}_I(\mathbf{x}) \mathbf{N}(\mathbf{x}) \mathbf{D}\mathbf{B}_J(\mathbf{x}) d\Gamma - \int_{\Gamma_{qu}} \mathbf{V}_I(\mathbf{x}) \mathbf{N}(\mathbf{x}) \mathbf{D}\mathbf{B}_J(\mathbf{x}) d\Gamma \tag{42}$$

$$\mathbf{F}(\mathbf{x},t) = \mathbf{F}^e(\mathbf{x},t) + \mathbf{F}^p(\mathbf{x},t) \tag{43}$$

where $\mathbf{F}^e(\mathbf{x},t)$ is the external force and $\mathbf{F}^p(\mathbf{x},t)$ is the internal force resulted in from plastic strain, respectively;

$$\mathbf{F}_I^e(\mathbf{x},t) = \int_{\Omega_q} \mathbf{b}_I(\mathbf{x},t) \mathbf{V}_I(\mathbf{x}) d\Omega + \int_{\Gamma_{qt}} \bar{\mathbf{t}}_I(\mathbf{x},t) \mathbf{V}_I(\mathbf{x}) d\Gamma \tag{44}$$

$$\mathbf{F}_I^p(\mathbf{x},t) = \int_{\Omega_q} \widehat{\mathbf{W}}_I^T(\mathbf{x}) \mathbf{D}\boldsymbol{\varepsilon}^p(\mathbf{x},t) \mathbf{x} d\Omega - \int_{\Gamma_{qi}} \mathbf{V}_I(\mathbf{x}) \mathbf{N}(\mathbf{x}) \mathbf{D}\boldsymbol{\varepsilon}^p(\mathbf{x},t) \mathbf{x} d\Gamma - \int_{\Gamma_{qu}} \mathbf{V}_I(\mathbf{x}) \mathbf{N}(\mathbf{x}) \mathbf{D}\boldsymbol{\varepsilon}^p(\mathbf{x},t) \mathbf{x} d\Gamma \tag{45}$$

where $\mathbf{V}_I(\mathbf{x})$, $\widehat{\mathbf{W}}_I^T$, $\mathbf{b}_I(\mathbf{x},t)$ and $\bar{\mathbf{t}}_I(\mathbf{x},t)$ are the test function, test function derivatives, body force and surface traction matrices, corresponding to node i, respectively.

$$\mathbf{V}_I = \begin{bmatrix} v(\mathbf{x},\mathbf{x}_I) & 0 & 0 \\ 0 & v(\mathbf{x},\mathbf{x}_I) & 0 \\ 0 & 0 & v(\mathbf{x},\mathbf{x}_I) \end{bmatrix} \tag{46}$$

$$\widehat{\mathbf{W}}_I = \begin{bmatrix} v_{,x}(\mathbf{x},\mathbf{x}_I) & 0 & 0 & v_{,y}(\mathbf{x},\mathbf{x}_I) & 0 & v_{,z}(\mathbf{x},\mathbf{x}_I) \\ 0 & v_{,y}(\mathbf{x},\mathbf{x}_I) & 0 & v_{,x}(\mathbf{x},\mathbf{x}_I) & v_{,z}(\mathbf{x},\mathbf{x}_I) & 0 \\ 0 & 0 & v_{,z}(\mathbf{x},\mathbf{x}_I) & 0 & v_{,y}(\mathbf{x},\mathbf{x}_I) & v_{,x}(\mathbf{x},\mathbf{x}_I) \end{bmatrix} \tag{47}$$

Equations similar to Eq. 41 with mass, stiffness and force matrix (as Eqs. 42-46) are obtained for each cubic local sub-domain Ω_q, whose centre is at the node $\mathbf{x}_I$. The Gauss quadrature rule of an appropriate order is employed to evaluate integrals over each local sub-domain.

The Newmark β method [Newmark (1959)], well known and commonly applied in computations, is used in the present study to integrate the governing equations

in time. This method assumes that the acceleration varies linearly within the time interval of $(t,\ t+\Delta t)$. The recursive relation among displacements, velocities and accelerations at times t and $t+\Delta t$ are;

$$\widehat{\mathbf{u}}^{t+\Delta t} = \widehat{\mathbf{u}}^{t} + \Delta t \dot{\widehat{\mathbf{u}}}^{t} + \frac{\Delta t^2}{2}\left[(1-2\beta)\ddot{\widehat{\mathbf{u}}}^{t} + 2\beta\ddot{\widehat{\mathbf{u}}}^{t+\Delta t}\right] \tag{48}$$

$$\dot{\widehat{\mathbf{u}}}^{t+\Delta t} = \dot{\widehat{\mathbf{u}}}^{t} + \Delta t\left[(1-\gamma)\ddot{\widehat{\mathbf{u}}}^{t} + \gamma\ddot{\widehat{\mathbf{u}}}^{t+\Delta t}\right] \tag{49}$$

Where $\widehat{\mathbf{u}}$, $\dot{\widehat{\mathbf{u}}}$, $\ddot{\widehat{\mathbf{u}}}$ are the fictitious nodal displacements, velocities and accelerations, respectively. β and γ are constant, for zero damping system, this method is unconditionally stable if;

$$2\beta \geq \gamma \geq \frac{1}{2} \tag{50}$$

and conditionally stable if;

$$\gamma \geq \frac{1}{2} \quad \beta \geq \frac{1}{2} \tag{51}$$

$$\Delta \mathrm{t} \leq \frac{1}{\omega_{\max}\sqrt{\frac{\gamma}{2}-\beta}} \tag{52}$$

where ω_{max} is the maximum frequency at the quadrature points. The value of ω_{max}depends on the size of local support domains and the size of local quadrature domains [Belytschko, Guo, Liu and Xiao (2000)] .

It can be seen that the response at time $t+\Delta t$ is obtained by evaluating the equation of motion at time $t+\Delta t$, therefore, the Newmark method is an implicit method. By setting $\beta = 1/4\,\gamma = 1/2$ it results in the constant acceleration scheme. It is non-dissipative, second-order accurate and unconditionally stable. Writing Eq. 41 at time $t+\Delta t$, and substituting from Eqs. 49 and 50 give the following system of algebraic equations;

$$\widehat{\mathbf{K}}(\mathbf{x},t)\,\widehat{\mathbf{u}}^{t+\Delta t} = \widehat{\mathbf{F}}^{t+\Delta t}(\mathbf{x},t) \tag{53}$$

where,

$$\widehat{\mathbf{K}}(\mathbf{x},t) = \mathbf{K}(\mathbf{x}) + \frac{4}{\Delta \mathrm{t}^2}\mathbf{M}(\mathbf{x}) \tag{54}$$

and,

$$\widehat{\mathbf{F}}(\mathbf{x},t) = \mathbf{F}^{t+\Delta t}(\mathbf{x},t) + \mathbf{M}(\mathbf{x}) \left(\frac{4}{\Delta t^2} \widehat{\mathbf{u}}^t + \frac{4}{\Delta t} \dot{\widehat{\mathbf{u}}}^t + \ddot{\widehat{\mathbf{u}}}^t \right) \tag{55}$$

having computed $\widehat{\mathbf{u}}^{t+\Delta t}$ from Eq. 54, $\dot{\widehat{\mathbf{u}}}^{t+\Delta t}$ and $\ddot{\widehat{\mathbf{u}}}^{t+\Delta t}$ are obtained from;

$$\ddot{\widehat{\mathbf{u}}}^{t+\Delta t} = \frac{4}{\Delta t^2} \left(\widehat{\mathbf{u}}^{t+\Delta t} - \widehat{\mathbf{u}}^t \right) - \frac{4}{\Delta t} \dot{\widehat{\mathbf{u}}}^t - \ddot{\widehat{\mathbf{u}}}^t \tag{56}$$

$$\dot{\widehat{\mathbf{u}}}^{t+\Delta t} = \dot{\widehat{\mathbf{u}}}^t + \frac{\delta t}{2} \left(\ddot{\widehat{\mathbf{u}}}^t + \ddot{\widehat{\mathbf{u}}}^{t+\Delta t} \right) \tag{57}$$

To enforce essential boundary conditions, the direct interpolation method is used [Liu, G. R. and Gu (2005)] . Note that, in MLPG, the system equation is constructed node by node. There are only three rows in the global stiffness matrix and the global force vector that are related to each field node in 3D formulation. With this structural feature of the system equation of MLPG, the following procedure can be implemented.

Assume the displacements at the Ith field node on the essential boundary are prescribed as;

$$\begin{cases} \left[u_x^h(\mathbf{x},t)\right]^I = \overline{u}_x^I(\mathbf{x},t) \\ \left[u_y^h(\mathbf{x},t)\right]^I = \overline{u}_y^I(\mathbf{x},t) \\ \left[u_z^h(\mathbf{x},t)\right]^I = \overline{u}_z^I(\mathbf{x},t) \end{cases} \tag{58}$$

where $u_x^h(\mathbf{x},t)$ $u_y^h(\mathbf{x},t)$ and $u_z^h(\mathbf{x},t)$ are approximated displacements in x, y and z direction, respectively. Using the MLS approximation, one has,

$$\begin{aligned} \left[u^h(\mathbf{x},t)\right]^I &= \begin{pmatrix} \left[u_x^h(\mathbf{x},t)\right]^I \\ \left[u_y^h(\mathbf{x},t)\right]^I \\ \left[u_z^h(\mathbf{x},t)\right]^I \end{pmatrix} \\ &= \begin{pmatrix} \Phi_1(\mathbf{x}) & 0 & 0 & \dots & \Phi_n(\mathbf{x}) & 0 & 0 \\ 0 & \Phi_1(\mathbf{x}) & 0 & \dots & 0 & \Phi_n(\mathbf{x}) & 0 \\ 0 & 0 & \Phi_1(\mathbf{x}) & \dots & 0 & 0 & \Phi_n(\mathbf{x}) \end{pmatrix} \begin{pmatrix} \hat{u}_x^1(t) \\ \hat{u}_y^1(t) \\ \hat{u}_z^1(t) \\ \vdots \\ \hat{u}_x^n(t) \\ \hat{u}_y^n(t) \\ \hat{u}_z^n(t) \end{pmatrix} \\ &= \mathbf{\Phi}(\mathbf{x}) \widehat{\mathbf{u}}(t) = \begin{pmatrix} \overline{u}_x^I(\mathbf{x},t) \\ \overline{u}_y^I(\mathbf{x},t) \\ \overline{u}_z^I(\mathbf{x},t) \end{pmatrix} \end{aligned} \tag{59}$$

where n is number of nodes in the support domain of the Ith node. Equation (60) produces three linear equations for the Ith field node, and can be rewritten explicitly as;

$$\begin{cases} \Phi_1(\mathbf{x})\,\hat{u}_x^1(t) + \Phi_2(\mathbf{x})\,\hat{u}_x^2(t) + \cdots + \Phi_n(\mathbf{x})\,\hat{u}_x^n(t) = \overline{u}_x^I(\mathbf{x},t) \\ \Phi_1(\mathbf{x})\,\hat{u}_y^1(t) + \Phi_2(\mathbf{x})\,\hat{u}_y^2(t) + \cdots + \Phi_n(\mathbf{x})\,\hat{u}_y^n(t) = \overline{u}_y^I(\mathbf{x},t) \\ \Phi_1(\mathbf{x})\,\hat{u}_z^1(t) + \Phi_2(\mathbf{x})\,\hat{u}_z^2(t) + \cdots + \Phi_n(\mathbf{x})\,\hat{u}_z^n(t) = \overline{u}_z^I(\mathbf{x},t) \end{cases} \tag{60}$$

Equation (61) is assembled directly into the system equations for the field nodes to obtain the modified global system equations of,

$$\widehat{\mathbf{K}}_{\mathrm{c}}(\mathbf{x},t)\,\widehat{\mathbf{u}}^{t+\Delta t} = \widehat{\mathbf{F}}_{\mathrm{c}}^{t+\Delta t}(\mathbf{x},t) \tag{61}$$

where $\widehat{\mathbf{K}}_{\mathrm{c}}(\mathbf{x},t)$ and $\widehat{\mathbf{F}}_{\mathrm{c}}^{t+\Delta t}(\mathbf{x},t)$ are modified global stiffness matrix and force vector, respectively.

Due to the nonlinearities involved in the internal force resulted in from plastic strain, Eq. 62 cannot be solved directly. Accordingly, an incremental approach is implemented to solve the mentioned equation. Thereby, the displacement, plastic strain and external force terms are written as increments so that;

$$\widehat{\mathbf{K}}_{\mathrm{c}}(\mathbf{x},t)\,d\widehat{\mathbf{u}}^{t+\Delta t} = d\widehat{\mathbf{F}}_{\mathrm{c}}^{t+\Delta t}(\mathbf{x},t) \tag{62}$$

$$\widehat{\mathbf{u}}_{k+1} = \widehat{\mathbf{u}}_k + d\widehat{\mathbf{u}}_{k+1} \tag{63}$$

$$\varepsilon_{k+1}^p = \varepsilon_k^p + d\boldsymbol{\varepsilon}_{k+1}^p \tag{64}$$

$$\boldsymbol{\sigma}_{k+1} = \boldsymbol{\sigma}_k + d\boldsymbol{\sigma}_{k+1} \tag{65}$$

where in each time increment, displacement, plastic strain and stress will be updated iteratively.

5 Numerical examples

Several numerical examples are considered to illustrate the accuracy and efficiency of the present method. In all the cases, results obtained from present MLPG formulation are compared with those of finite element solution from ABAQUS.

Gauss quadrature is implemented for numerical integration of governing equations. For each Gauss quadrature point $\mathbf{x}_q$, the MLS shape functions are constructed in

the domain of Ω_q to obtain the integrand. Cubic quadrature domain is used to integrate the integral equations. For node $\mathbf{x}_I$, the size of quadrature domain in x direction can be determined by $r_q^x = \alpha_{qx} d_I^x$, where those for y and z directions are obtained by substituting x with y and z, respectively. Herein, α_{qx} is dimensionless size of the local quadrature domain in the x direction. Accordingly, α_{qy} and α_{qz} are dimensionless sizes of the local quadrature domain in the y and z directions, respectively.

The local support domain for a Gauss quadrature point $\mathbf{x}_q$ can be arbitrary in shape. In this paper, a cubic support domain is used. The size of the local support domain in x direction is determined by $r_s^x = \alpha_{sx} d_I^x$, where those for y and z directions are obtained by substituting x with y and z, respectively. Herein, α_{sx} is dimensionless size of the local support domain in the x direction. Accordingly, α_{sy} and α_{sz} are dimensionless sizes of the local support domain in the y and z directions, respectively.

where d_I^x, d_I^y and d_I^z are the local nodal spacing in x, y and z directions, respectively.

In this regard, the dimensions of the local quadrature domain and local support domain used for Gauss quadrature and constructing the MLS shape functions become $(2\alpha_{qx} d_I^x) \times (2\alpha_{qy} d_I^y) \times (2\alpha_{qz} d_I^z)$ and $(2\alpha_{sx} d_I^x) \times (2\alpha_{sy} d_I^y) \times (2\alpha_{sz} d_I^z)$, respectively. In the present study, for the local support domain, $\alpha_{sx} = \alpha_{sy} = \alpha_{sz} = 2.7$ and for the local quadrature domain, $\alpha_{qx} = \alpha_{qy} = \alpha_{qz} = 0.8$ are used.

5.1 Dynamic analysis of a 3D cantilever plate

A 3D cantilever plate subjected to an instantaneously uniformly distributed step load *600g(t)* is analyzed. Fig. 2 shows the geometry and 3D discretization of the plate. The applied loading history can be seen in Fig. 3a. The linear work hardening stress-strain relation is considered for the plate's material (Fig. 3b). The plate thickness to span ratio is *h/a=0.1*. In the present example, the following material constants are considered: Young's modulus $E=2.1\times10^{11}$ *pa*, Poisson's ratio $\nu=0.3$, mass density $\rho=1000$ *kg/m*^{3}, yield stress $\sigma_0=1.7\times10^5$*pa* and work hardening modulus $E_T=2\times10^{10}$ *pa*. Due to symmetry, only one half of the plate is discretized by the $7\times3\times3$ uniformly distributed nodal points on the domain of the plate.

Fig. 4 depicts the elasto-plastic time history of the transverse displacement at the end point on the mid-line of the plate. In this figure the results obtained from the present method are compared with those computed from finite element commercial software ABAQUS with 6250 C3D8R elements in one half of plate. It can be seen that the obtained results from the present meshless method are in good agreement with those of FEM with much lesser number of nodes in the problem domain.

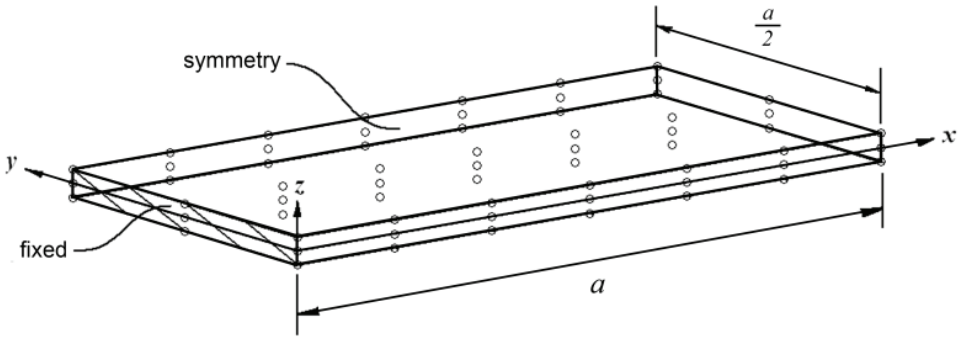

Figure 2: Geometry and discretization of the cantilever plate.

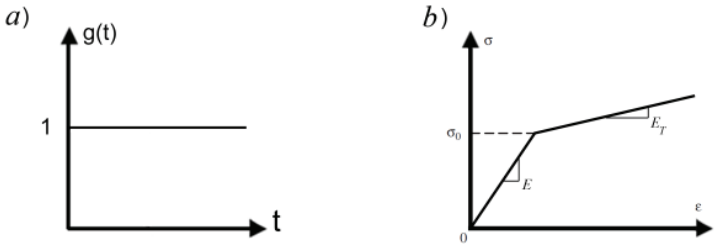

Figure 3: a) Applied load history, b) linear work hardening stress-strain curve.

Elastic and elasto-plastic time history of the plate are also exhibited in the Fig. 5. In this figure, the permanent effects of plastic strains are clearly demonstrated.

5.2 Dynamic analysis of a 3D fully clamped plate

Consider a fully clamped square plate of length a and thickness h made of linear work hardening material subjected to a suddenly applied uniform loads *8000g(t)* and *10000g(t)*. The plate thickness to span ratio is *0.1* and its material properties are $E=10\times10^5\ pa$, $\nu=0.3$, $\rho=1000\ kg/m^3$, $\sigma_0=2.7\times10^4 pa$ and $E_T=1\times10^5 pa$. Due to symmetry, only one quarter of the plate is discretized by $9\times9\times3$ nodes on the problem domain and is shown in Fig. 6.

Fig. 7 and 8 present elasto-plastic time history of the transverse displacement at the midpoint of the plate for applied loads of *8000g(t)* and *10000g(t),* respectively. It is clear that with the increase of applied loading amplitude, the permanent effects of plastic strains on the plate deflection are enhanced. In this example, the

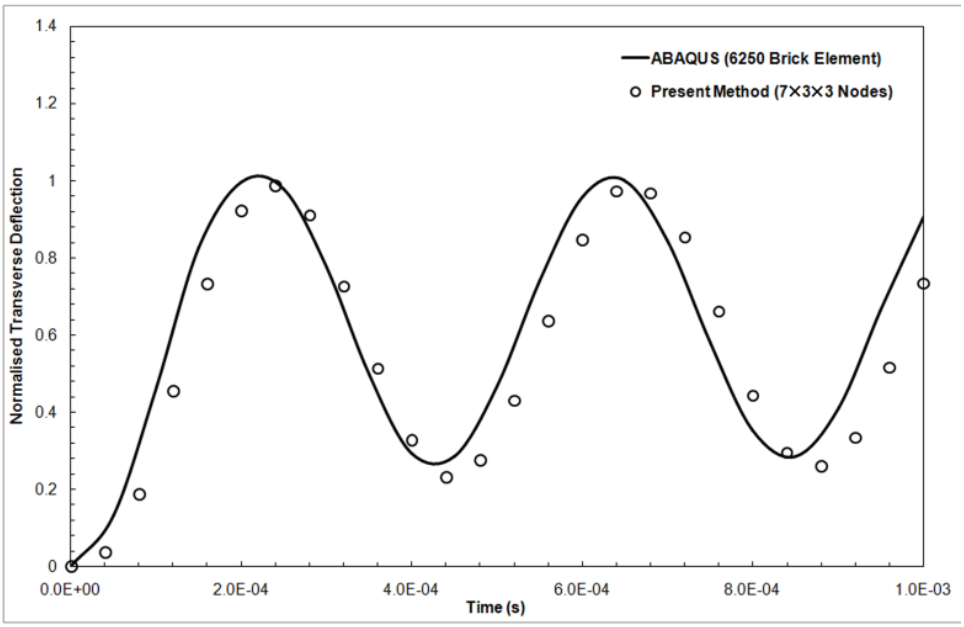

Figure 4: Elasto-plastic time history of the transverse displacement at the end point on the mid-line of the plate.

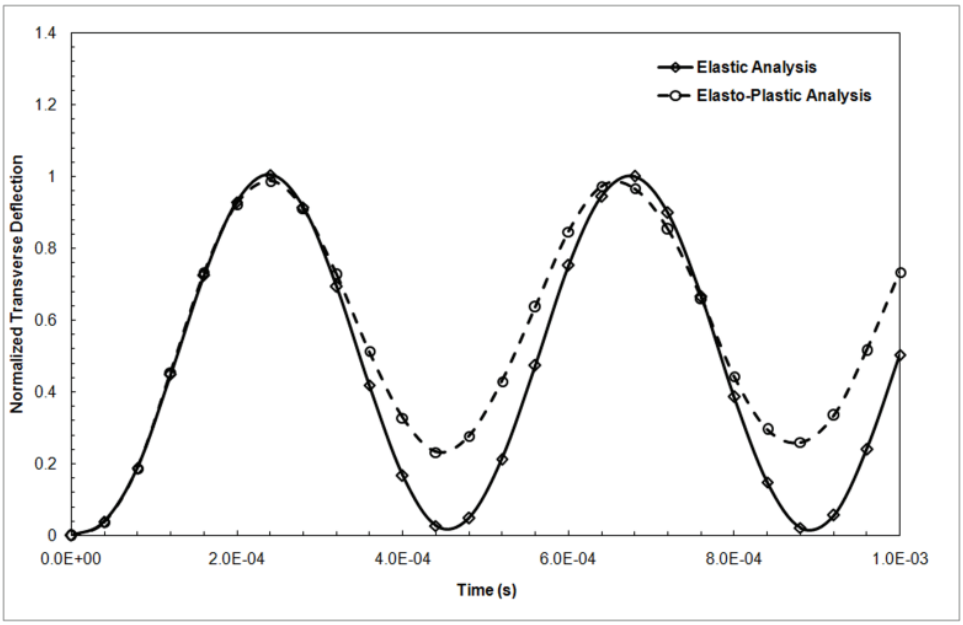

Figure 5: Elastic and elasto-plastic response of the cantilever plate.

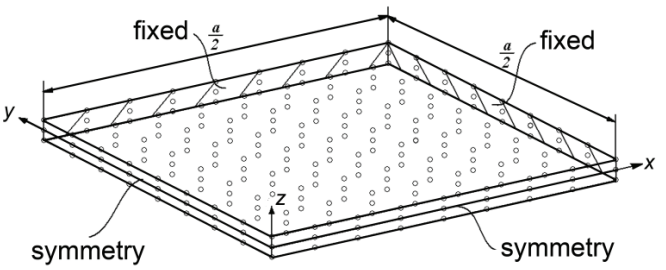

Figure 6: Discretization of one quarter of the plate with $9\times9\times3$ nodes.

results obtained from present meshless method are also compared with those of FEM from ABAQUS with 6250 C3D8R elements in one quarter of plate and are in good agreement with them. Fig. 9 shows the elastic and elasto-plastic time history of the transverse displacement of the plate with applied load of *10000g(t)*.

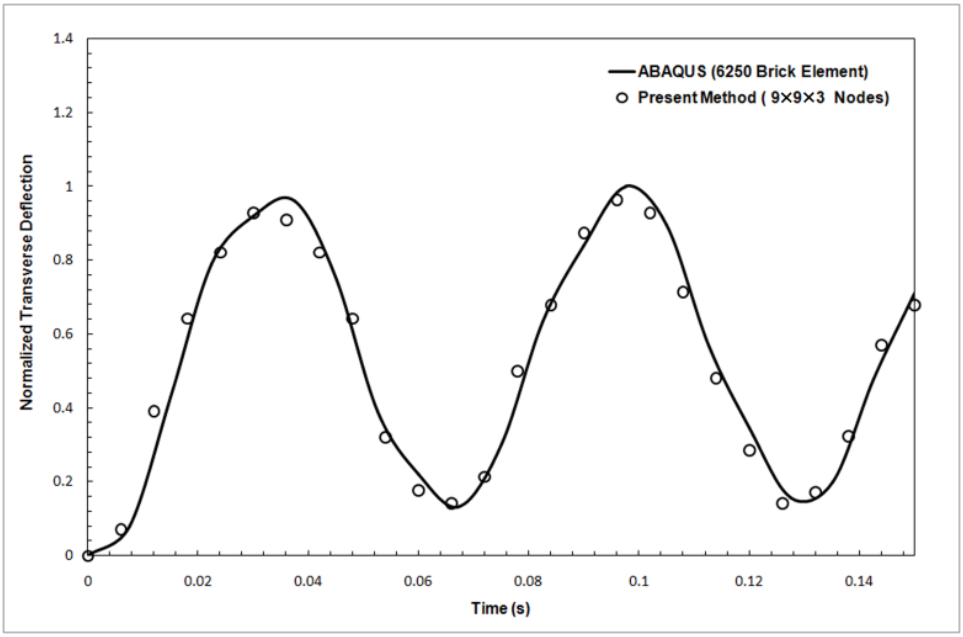

Figure 7: Elasto-plastic time history of the transverse displacement of the fully clamped plate at its midpoint with applied load of *8000g(t)*.

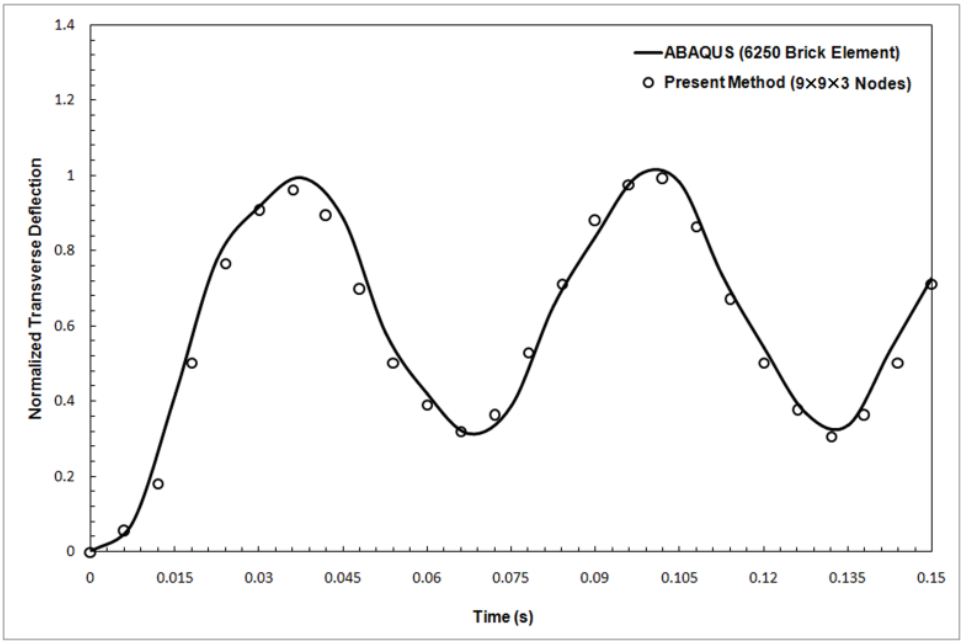

Figure 8: Elasto-plastic time history of the transverse displacement of the fully clamped plate at its midpoint with applied load of *10000g(t)*.

6 Conclusion

The meshless local Petrov-Galerkin method is developed for nonlinear dynamic elasto-plastic analysis of 3D problems. Based on local Petrov-Galerkin approach, weak form of equilibrium equation is obtained. Nodal points are distributed in the 3D analyzed domain and each node is surrounded by a cubic sub-domain to which a local integral equation is applied. Three dimensional Moving Least-Square (MLS) approximation is used as shape function to get the meshless discrete system of equations. Numerical integration is performed using Gauss quadrature method. A weak formulation for the set of governing equations is transformed into local integral equations on local sub-domains by using a unit test function. Fourth-order spline function is used as the weight function as well as the test function. Stress-strain relation in elasto-plasticity problems is represented based on normality hypothesis of plasticity and the unknown plastic multiplier is obtained by the consistency condition. Von Mises yield criterion in three dimensional space is used as a yield function to determine whether the material has yielded. The final nonlinear Ordinary Differential Equations (ODEs) of the problem domain are solved by the Newmark time integration method in an incremental form. Several numeri-

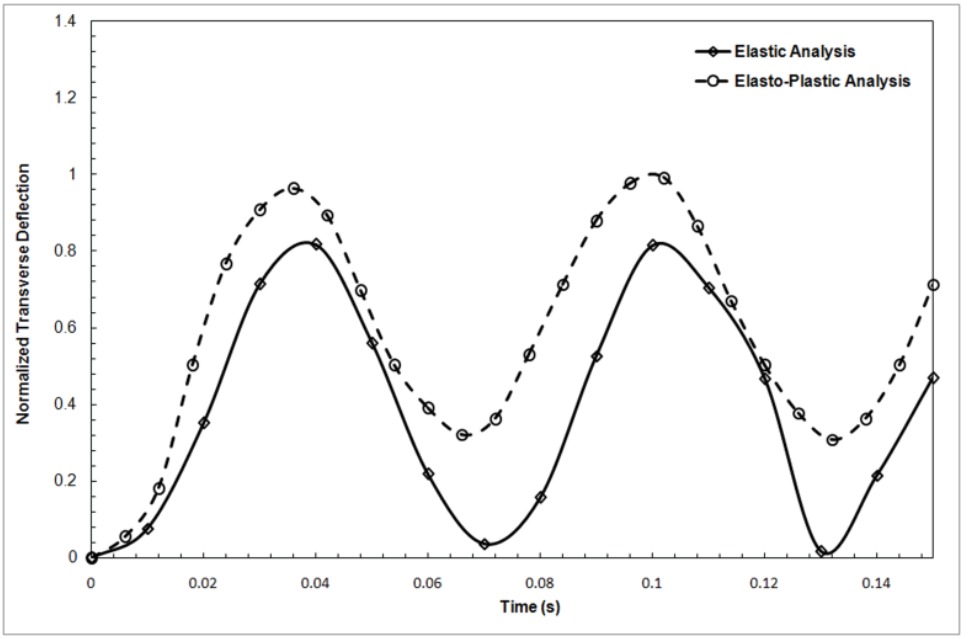

Figure 9: Elastic and elasto-plastic response of the fully clamped plate with applied load of *10000g(t)*.

cal examples are presented to illustrate the effectiveness of present formulation for the elasto-plastic analysis of 3D solids subjected to dynamic loading. It has been found that this meshless method is very effective with much lesser number of nodes in comparison to FEM.

Reference

Atluri, S. N.; Cho, J. Y.; Kim, H. G. (1999): Analysis of thin beams, using the meshless local Petrov–Galerkin method, with generalized moving least squares interpolations. *CMES: Computer Modeling in Engineering & Sciences,* vol. 24, no. pp. 334-347.

Atluri, S. N.; Kim, H. G.; Cho, J. Y. (1999): A critical assessment of the truly meshless local Petrov–Galerkin (MLPG), and local boundary integral equation (LBIE) methods. *Comput. Mech.,* vol. 24, no. pp. 348-372.

Atluri, S. N.; Shen, S. (2002a): The meshless local Petrov-Galerkin (MLPG) method: A simple & less costly alternative to the finite element and boundary element methods. *CMES: Computer Modeling in Engineering & Sciences,* vol. 3, no.

pp. 11-52.

Atluri, S. N.; Shen, S. (2002b): *The Meshless Local Petrov–Galerkin (MLPG) Method*. Tech Science Press

Atluri, S. N.; Zhu, T. (1998): A new meshless local Petrov–Galerkin (MLPG) approach in computational mechanics. *Comput. Mech.,* vol. 22, no. pp. 117-127.

Atluri, S. N.; Zhu, T. (2000): The meshless local Petrov–Galerkin (MLPG) approach for solving problems in elasto-statics. *Comput. Mech.,* vol. 25, no. pp. 169-179.

Babuska, I.; Melenk, J. (1997): The partition of unity method. *int. J. Numer. Methods Engrg.,* vol. 40, no. pp. 727–758.

Batra, R. C.; Ching, H. K. (2002): Analysis of elastodynamic deformation near a crack/ notch tip by the meshless local Petrov–Galerkin (MLPG) Method. *CMES: Computer Modeling in Engineering & Sciences,* vol. 3, no. pp. 717-730.

Belytschko, T.; Guo, Y.; Liu, W. K.; Xiao, S. P. (2000): A unified stability of meshless particle methods. *Int. J. Numer. Methods Engrg.,* vol. 48, no. pp. 1359-1400.

Belytschko, T.; Lu, Y. Y.; Gu, L. (1994): Element-free Galerkin methods. *Int. J. Numer. Methods Engrg.,* vol. 37, no. pp. 229-256.

Ching, H. K.; Batra, R. C. (2001): Determination of crack tip fields in linear elastostatics by the meshless local Petrov–Galerkin (MLPG) method. *CMES: Computer Modeling in Engineering & Sciences,* vol. 2, no. pp. 273-290.

Ching, H. K.; Yen, S. C. (2005): Meshless local Petrov-Galerkin analysis for 2D functionally graded elastic solids under mechanical and thermal loads. *Composites: Part B,* vol. 36, no. pp. 223-240.

Ching, H. K.; Yen, S. C. (2006): Transient thermoelastic deformations of 2-D functionally graded beams under nonuniformly convective heat supply. *Compos. Struct,* vol. 73, no. pp. 381-393.

Duarte, C. A.; Oden, J. T. (1996): An h–p adaptive method using clouds. *Comput. Methods Appl. Mech. Engrg. ,* vol. 139, no. pp. 237–262.

Gilhooley, D. F.; Batra, R. C.; Xiao, J. R.; McCarthy, M. A.; Gillespie Jr., J. W. (2007): Analysis of thick functionally graded plates by using higher-order shear and normal deformable plate theory and MLPG method with radial basis functions. *Compos. Struct,* vol. 80, no. pp. 539-552.

Gu, Y. T.; Liu, G. R. (2001): A meshless local Petrov–Galerkin (MLPG) formulation for static and free vibration analyses of thin plates. *CMES: Computer Modeling in Engineering & Sciences,* vol. 2, no. pp. 463-476.

Gu, Y. T.; Wang, Q. X.; Lam, K. Y.; Dai, K. Y. (2007): A pseudo-elastic local meshless method for analysis of material nonlinear problems in solids. *Eng. Anal. Bound. Elem.,* vol. 31, no. pp. 771-782.

Han, Z. D.; Atluri, S. N. (2004): Meshless Local Petrov-Galerkin (MLPG) approaches for solving 3D Problems in elasto-statics. *CMES: Computer Modeling in Engineering & Sciences,* vol. 6, no. pp. 168-188.

Han, Z. D.; Rajendran, A. M.; Atluri, S. N. (2005): Meshless Local Petrov-Galerkin (MLPG) Approaches for Solving Nonlinear Problems with Large Deformations and Rotations. *CMES: Computer Modeling in Engineering & Sciences,* vol. 10, no. pp. 1-12.

Heaney, C.; Augarde, C.; Deeks, A. (2009): Modelling Elasto-Plasticity Using the Hybrid MLPG Method. *CMES: Computer Modeling in Engineering & Sciences,* vol. 56, no. 2, pp. 153-178.

Kim, H. G.; Atluri, S. N. (2000): Arbitrary placement of secondary nodes, and error control, in the meshless local Petrov–Galerkin (MLPG) method. *CMES: Computer Modeling in Engineering & Sciences,* vol. 1, no. pp. 11-32.

Li, Q.; Soric, J.; Jarak, T.; Atluri, S. N. (2005): A locking-free meshless local Petrov–Galerkin formulation for thick and thin plates. *J. Comput. Phys.,* vol. 208, no. pp. 116-133.

Lin, H.; Atluri, S. N. (2000): Meshless local Petrov–Galerkin (MLPG) method for convection-diffusion problems. *CMES: Computer Modeling in Engineering & Sciences,* vol. 1, no. pp. 45-60.

Lin, H.; Atluri, S. N. (2001): The meshless local Petrov–Galerkin (MLPG) method for solving incompressible Navier–Stokes equations. *CMES: Computer Modeling in Engineering & Sciences,* vol. 2, no. pp. 117-142.

Liu, G. R.; Gu, Y. T. (2005): *An Introduction to Meshfree Methods and Their Programming*. Springer

Liu, W. K.; Jun, S.; Zhang, Y. (1995): Reproducing kernel particle methods. *Int. J. Numer. Methods in Fluids,* vol. 20, no. pp. 1081-1106.

Long, S.; Atluri, S. N. (2002): A meshless local Petrov–Galerkin (MLPG) method for solving the bending problem of a thin plate. *CMES: Computer Modeling in Engineering & Sciences,* vol. 3, no. pp. 53-64.

Long, S. Y.; Liu, K. Y.; Li, G. Y. (2008): An analysis for the elasto-plastic fracture problem by the meshless local Petrov-Galerkin method. *CMES: Computer Modeling in Engineering & Sciences,* vol. 28, no. pp. 203-216.

Lucy, L. B. (1977): A numerical approach to the testing of the fission hypothesis. *Astronom. J.,* vol. 82, no. pp. 1013–1024.

Nayroles, B.; Touzot, G.; Villon, P. (1992): Generalizing the finite element method: diffuse approximation and diffuse elements. *Comput. Mech. ,* vol. 10, no. pp. 307–18.

Newmark, N. M. (1959): A method of computation for structural dynamics. *J. Eng. Mech. Div.-ASCE,* vol. 85, no. pp. 67-94.

Qian, L. F.; Batra, R. C.; Chen, L. M. (2003): Elastostatic Deformations of a Thick Plate by using a Higher-Order Shear and Normal Deformable Plate Theory and two Meshless Local Petrov-Galerkin (MLPG) Methods. *CMES: Computer Modeling in Engineering & Sciences,* vol. 4, no. pp. 161-175.

Qian, L. F.; Batra, R. C.; Chena, L. M. (2004): Static and dynamic deformations of thick functionally graded elastic plates by using higher-order shear and normal deformable plate theory and meshless local Petrov–Galerkin method. *Composites: Part B,* vol. 35, no. pp. 685-697.

Rezaei Mojdehi, A.; Darvizeh, A.; Basti, A. (2011): Application of Meshless Local Petrov-Galerkin (MLPG) Method to Three Dimensional Elasto-Plastic Problems based on Deformation Theory of Plasticity. *CMES: Computer Modeling in Engineering & Sciences,* vol. 77, no. pp. 1-31.

Rezaei Mojdehi, A.; Darvizeh, A.; Basti, A.; Rajabi, H. (2011): Three dimensional static and dynamic analysis of thick functionally graded plates by the meshless local Petrov–Galerkin (MLPG) method. *Eng. Anal. Bound. Elem. ,* vol. 35, no. pp. 1168-1180.

Sladek, J.; Sladek, V.; Atluri, S. N. (2001): A pure contour formulation for the meshless local boundary intergral equation method in thermoelasticity. *CMES: Computer Modeling in Engineering & Sciences,* vol. 2, no. pp. 423-433.

Sladek, J.; Sladek, V.; Krivacek, J.; Wen, P. H.; Zhang, C. h. (2007): Meshless local Petrov–Galerkin (MLPG) method for Reissner–Mindlin plates under dynamic load. *Comput. Methods Appl. Mech. Engrg.,* vol. 196, no. pp. 2681-2691.

Sladek, J.; Sladek, V.; Solek, P. (2009): Elastic analysis in 3D anisotropic functionally graded solids by the MLPG. *Comput. Methods Appl. Mech. Engrg.,* vol. 43, no. pp. 223-251.

Sladek, J.; sladek, V.; Zhang, C. h. (2005): Stress analysis in anisotropic functionally graded materials by the MLPG method. *Eng. Anal. Bound. Elem. ,* vol. 29, no. pp. 597-609.

Soares, D.; Sladek, J.; Sladek, V. (2009): Dynamic Analysis by Meshless Local Petrov-Galerkin Formulations Considering a Time-Marching Scheme Based on Implicit Green's Functions. *CMES: Computer Modeling in Engineering & Sciences,* vol. 50, no. pp. 115-140.

Soric, J.; Li, Q.; Jarak, T.; Atluri, S. N. (2004): Meshless Local Petrov-Galerkin (MLPG) Formulation for Analysis of Thick Plates. *CMES: Computer Modeling in Engineering & Sciences,* vol. 6, no. pp. 349-357.

Sukumar, N.; Moran, B.; Belytschko, T. (1998): The natural element method in solid mechanics. *Int. J. Numer. Methods Engrg.,* vol. 43, no. pp. 839–887.

Tang, Z.; Shen, S.; Atluri, S. N. (2003): Analysis of materials with strain-gradient effects: A meshless local Petrov–Galerkin (MLPG) approach, with nodal displacements only. *CMES: Computer Modeling in Engineering & Sciences,* vol. 4, no. pp. 177-196.

Wendland, H. (1995): Piecewise polynomial positive definite and compactly supported radial basis functions of minimal degree. *Adv. Comput. Methods,* vol. 4, no. pp. 389–396.

Xiao, J. R.; Batra, R. C.; Gilhooley, D. F.; Gillespie Jr., J. W.; McCarthy, M. (2007): Analysis of thick plates by using a higher-order shear and normal deformable plate theory and MLPG method with radial basis functions. *Comput. Methods Appl. Mech. Engrg.,* vol. 196, no. pp. 979-987.

Zhang, G. M.; Batra, R. C. (2004): Modified smoothed particle hydrodynamics method and its application to transient problems. *Comput. Mech.,* vol. 34, no. pp. 137- 46.

Zhang, X.; Zhenhan, Y.; Zhangfei, Z. (2006): Application of MLPG in large deformation analysis. *Acta Mech. Sin.,* vol. 22, no. pp. 331-340.